AIP Journal of Applied Physics

Role of substrate quality on the performance of semipolar (112¯2) InGaN light-emitting diodes

Duc V. Dinh, Brian Corbett, Peter J. Parbrook, Ingrid. L. Koslow, Monir Rychetsky, Martin Guttmann, Tim Wernicke, Michael Kneissl, Christian Mounir, Ulrich Schwarz, Johannes Glaab, Carsten Netzel, Frank Brunner, and Markus Weyers

Citation: Journal of Applied Physics **120**, 135701 (2016); doi: 10.1063/1.4963757
View online: http://dx.doi.org/10.1063/1.4963757
View Table of Contents: http://scitation.aip.org/content/aip/journal/jap/120/13?ver=pdfcov
Published by the AIP Publishing

Role of substrate quality on the performance of semipolar $(11\bar{2}2)$ InGaN light-emitting diodes

Duc V. Dinh,[1,a)] Brian Corbett,[1] Peter J. Parbrook,[1,2] Ingrid. L. Koslow,[3] Monir Rychetsky,[3] Martin Guttmann,[3] Tim Wernicke,[3] Michael Kneissl,[3] Christian Mounir,[4] Ulrich Schwarz,[5] Johannes Glaab,[6] Carsten Netzel,[6] Frank Brunner,[6] and Markus Weyers[6]

[1]*Tyndall National Institute, University College Cork, Lee Maltings, Dyke Parade, Cork, Ireland*
[2]*School of Engineering, University College Cork, Cork, Ireland*
[3]*Institut für Festkörperphysik, Technische Universität Berlin, Hardenbergstraße 36, 10623 Berlin, Germany*
[4]*Institut für Mikrosystemtechnik, Albert-Ludwigs-Universität Freiburg, Georges-Köhler-Allee 103, 79110 Freiburg, Germany*
[5]*Institut für Physik, Technische Universität Chemnitz, Reichenhainer Straße 70, 09126 Chemnitz, Germany*
[6]*Ferdinand-Braun-Institut, Leibniz-Insitut für Höchstfrequenztechnik, Gustav-Kirchhoff-Straße 4, 12489 Berlin, Germany*

(Received 5 August 2016; accepted 16 September 2016; published online 3 October 2016)

We compare the optical properties and device performance of unpackaged InGaN/GaN multiple-quantum-well light-emitting diodes (LEDs) emitting at ~430 nm grown simultaneously on a high-cost small-size bulk semipolar $(11\bar{2}2)$ GaN substrate (Bulk-GaN) and a low-cost large-size $(11\bar{2}2)$ GaN template created on patterned $(10\bar{1}2)$ *r*-plane sapphire substrate (PSS-GaN). The Bulk-GaN substrate has the threading dislocation density (TDD) of $\sim 10^5\,cm^{-2}$–$10^6\,cm^{-2}$ and basal-plane stacking fault (BSF) density of $0\,cm^{-1}$, while the PSS-GaN substrate has the TDD of $\sim 2\times 10^8\,cm^{-2}$ and BSF density of $\sim 1\times 10^3\,cm^{-1}$. Despite an enhanced light extraction efficiency, the LED grown on PSS-GaN has two-times lower internal quantum efficiency than the LED grown on Bulk-GaN as determined by photoluminescence measurements. The LED grown on PSS-GaN substrate also has about two-times lower output power compared to the LED grown on Bulk-GaN substrate. This lower output power was attributed to the higher TDD and BSF density. *Published by AIP Publishing.* [http://dx.doi.org/10.1063/1.4963757]

I. INTRODUCTION

Visible group III-nitride based light-emitting diodes (LEDs) employ indium-containing quantum wells (QWs) such as InGaN or In(Ga,Al)N in the active region. It is well-known that for polar (0001) *c*-plane QWs, the strong polarization-related electric fields along the [0001] direction cause a severe tilt of the QW energy band-edges resulting in a quantum-confined Stark effect (QCSE).[1–3] In contrast, for semipolar planes, e.g., $(11\bar{2}2)$, these fields are significantly reduced, resulting in an increase of the radiative recombination probability, which may enhance the performance of LEDs based on semipolar nitrides. High efficiency green[4] and yellow[5] packaged $(11\bar{2}2)$ InGaN/GaN LEDs grown on low threading dislocation density (TDD $\sim 10^5\,cm^{-2}$–$10^6\,cm^{-2}$) high-cost bulk $(11\bar{2}2)$ GaN substrates (Bulk-GaN substrates) have recently been demonstrated. However, these substrates are very small ($\leq 1\,cm^2$).[6] Therefore, hetero-epitaxially grown $(11\bar{2}2)$ GaN templates on sapphire substrates continue to be of interest due to the much lower cost and larger substrate sizes available. Several approaches have been employed to produce $(11\bar{2}2)$ GaN either directly grown[7–9] or epitaxially laterally overgrown on $(10\bar{1}0)$ *m*-plane sapphire substrates.[10,11] However, a major disadvantage of these approaches is the potentially detrimental contribution of high threading dislocation density (TDD $\sim 10^9\,cm^{-2}$–$10^{10}\,cm^{-2}$) and high basal-plane stacking fault (BSF) density ($>10^5\,cm^{-1}$).

Recently, high quality $(11\bar{2}2)$ GaN templates have been grown on patterned $(10\bar{1}2)$ *r*-plane sapphire substrates (PSS-GaN substrates) by metalorganic vapour phase epitaxy (MOVPE).[12–14] MOVPE-grown PSS-GaN substrates have even been successfully demonstrated on 100-mm-diameter wafers.[13] The upscaling to a larger wafer diameter is part of the combined efforts toward high efficiency cost-cutting LEDs for solid-state lighting applications.[15] High external quantum efficiency (EQE) has been achieved for polar InGaN LEDs grown on patterned *c*-plane sapphire,[16–18] it is therefore expected that the PSS-GaN substrates can also enhance light extraction efficiency of overgrown $(11\bar{2}2)$ LEDs resulting in an increased EQE compared to LEDs grown on non-patterned substrates.[19] However, this prediction needs to be further confirmed experimentally.[19–21]

In this paper, we report semipolar $(11\bar{2}2)$ InGaN LEDs emitting at ~430 nm grown simultaneously on PSS- and Bulk-GaN substrates. The optical properties and performance of the LEDs were assessed.

II. EXPERIMENTAL DETAILS

Growth of $(11\bar{2}2)$ InGaN/GaN LEDs was performed simultaneously on PSS- and Bulk-GaN substrates (so-called PSS- and Bulk-LEDs, respectively) in an Aixtron 3×2 in. close-coupled showerhead MOVPE reactor. The 300-μm-thick Bulk-GaN substrate (TDD $\sim 10^5\,cm^{-2}$–$10^6\,cm^{-2}$; BSF density $= 0\,cm^{-1}$) was sliced from *c*-plane GaN bulk crystals grown by hydride vapour phase epitaxy at Mitsubishi Chemical Corporation.[6] The specular and optically

a)Electronic mail: duc.vn.dinh@gmail.com

transparent surface of this substrate was obtained by mechanical and chemical polishing. The MOVPE growth of the 6-μm-thick PSS-GaN on 600-μm-thick sapphire substrate is reported elsewhere.[13] The typical TDD and BSF density of the PSS-GaN substrate were estimated to be $\sim 2 \times 10^8\,cm^{-2}$ and $\sim 1 \times 10^3\,cm^{-1}$, respectively. The low TDD and BSF density of the PSS-GaN template were obtained due to their terminations at the buried $\{11\bar{2}0\}$ facets during the coalescence process.[12–14]

The LED structures consisted of 1.5-μm-thick Si-doped n-type GaN ($[Si] \approx 1 \times 10^{19}\,cm^{-3}$), 100-nm-thick n-$In_{0.01}Ga_{0.99}N$ ($[Si] \approx 1 \times 10^{17}\,cm^{-3}$), a three period InGaN/GaN (2.5 nm/6.5 nm) QW active region, 120-nm-thick Mg-doped p-type GaN ($[Mg] \approx 8 \times 10^{19}\,cm^{-3}$), and 15 nm heavily doped p-type GaN contact layer ($[Mg] \approx 3 \times 10^{20}\,cm^{-3}$). A schematic of the device structures is shown in the inset of Fig. 2. Details of the LED growth conditions are reported elsewhere.[21] The composition of the InGaN QW active region was examined using a PANalytical X'pert triple-axis high-resolution X-ray diffraction system with a CuKα_1 source. The In-content of the QWs was estimated to be about 14%. The surface morphology of the LEDs was investigated by Olympus XC30 Nomarski differential interference contrast microscopy (Figs. 1(a) and 1(b)) and Veeco MultiMode atomic force microscope (AFM) in tapping mode (Figs. 1(c) and 1(d)). The AFM images of both samples show typical undulations along the $[1\bar{1}00]$ M-direction induced by the anisotropic diffusion of group-III atoms on the $(11\bar{2}2)$ surface.[7–9,13,20–22] The Bulk-LED shows smoother morphology with a smaller root-mean square (rms) roughness of 3 nm ($50 \times 50\,\mu m^2$) than the PSS-LED (rms = 16 nm).

To investigate the optical properties of the samples, the samples were mounted in a closed-cycle cryostat equipped with a Sumitomo Cryogenics air-cooled compressor for temperature-dependent macro-photoluminescence (TD-PL) measurements. The temperature measurement was varied from 10 K to 400 K. The PL emission spectra were measured using a Horiba iHR320 spectrometer equipped with a monochromator and a thermoelectrically cooled Synapse Charge-Coupled Device (CCD) detector. The samples were excited using a continuous-wave (cw) blue-violet laser diode ($E_{ex} = 3.06$ eV) with excitation power densities (P_{ex}) of 2–15 W/cm^2. Additionally, the samples were also characterized at room temperature (RT) via a custom designed confocal PL microscope (μ-PL). An objective with a numerical aperture of 0.75 was used with a 10-μm-diameter pinhole in the collection optics to ensure a diffraction limited lateral spatial resolution below 300 nm. The emission was analyzed by a 55 cm focal length spectrometer equipped with a back-illuminated CCD detector. For μ-PL maps ($30 \times 30\,\mu m^2$), a cw ultra-violet laser diode ($E_{ex} = 3.30$ eV, $P_{ex} = 150$ kW/cm^2) was used as quasi-resonant excitation source, i.e., just below the GaN bandgap of 3.44 eV at RT.

To investigate the spectral characteristics and cw on-wafer output power (P_{opt}) of unpackaged LEDs, the samples were etched for 30 s in diluted HCl (HCl:DI = 1:3) prior to the metal deposition to remove any native oxide. $200 \times 200\,\mu m^2$ Ni/Au p-contacts (10/10 nm thick) were deposited in a thermal evaporator on the p-GaN layers. Following deposition, the p-contacts were annealed in a rapid thermal annealer at 545 °C under oxygen flow for 5 min. Afterwards, Ti/Au alloys (20/500 nm thick) were deposited on the Ni/Au p-contacts for reinforcement. Finally, $20 \times 20\,\mu m^2$ grids were formed on the Ti/Au reinforcement with lithography to use the p-contacts for transmission/reflectance measurements. Metallic In was used as a side n-contact to the n-GaN layer, i.e., there is no explicit n-contacts. RT macro-electroluminescence (RT-EL) measurements were performed in pulsed mode (5 μs pulse width and 0.5% duty cycle) at an injection current (I_{inject}) of 0–100 mA (the corresponding current density (J_{inject}) of 0–250 A/cm^2). P_{opt} of the LEDs was recorded on-wafer with needle probes (i.e., the light extraction is expected to be very low) in a direct-current (DC) mode inside a calibrated 50-cm-diameter integrating sphere to collect light emitted in all directions.

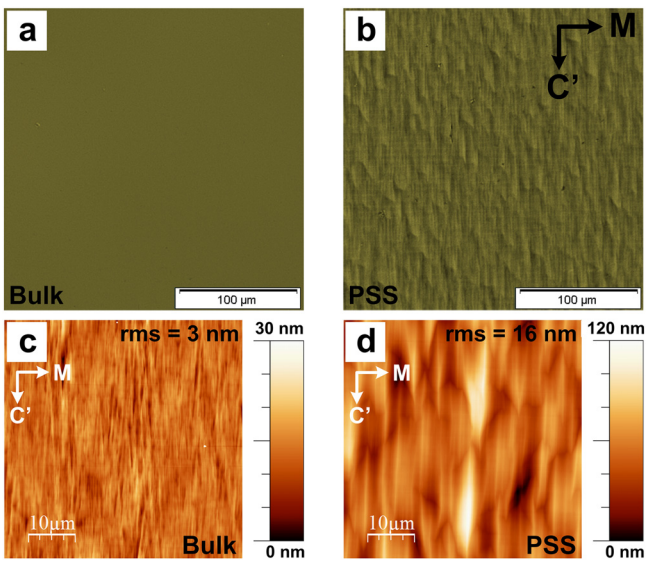

FIG. 1. (Top row) Nomarski images ($250 \times 250\,\mu m^2$) of the (a) Bulk-LED and (b) PSS-LED. (Bottom row) AFM images ($50 \times 50\,\mu m^2$) of the (c) Bulk-LED and (d) PSS-LED. The root-mean square (rms) roughness values of the samples were shown for comparison.

III. RESULTS AND DISCUSSION

A. Device performance

Figure 2 shows examples of current-voltage characteristic curves measured on five different $(11\bar{2}2)$ InGaN/GaN MQW LEDs. Despite the unprocessed n-contact, both the LED samples show typical p-n junction characteristics with a turn-on voltage of about 4.0 V. For fully processed LEDs, i.e., with processed n-/p-contacts, which were grown under the same conditions, the turn-on voltage was estimated to be $\sim$3.5 V.[21]

Figure 3(a) shows the RT-EL spectra of the $200 \times 200\,\mu m^2$ PSS-LED as a function of I_{inject} (J_{inject} = 0–250 A/cm^2). The peak emission wavelength (λ_{EL}) remains unchanged at about 430 nm over the whole range of $I(J)_{inject}$ applied. The photograph in the inset of Fig. 3(a) displays bright blue-emission from the PSS-LED at 20 mA driven current.

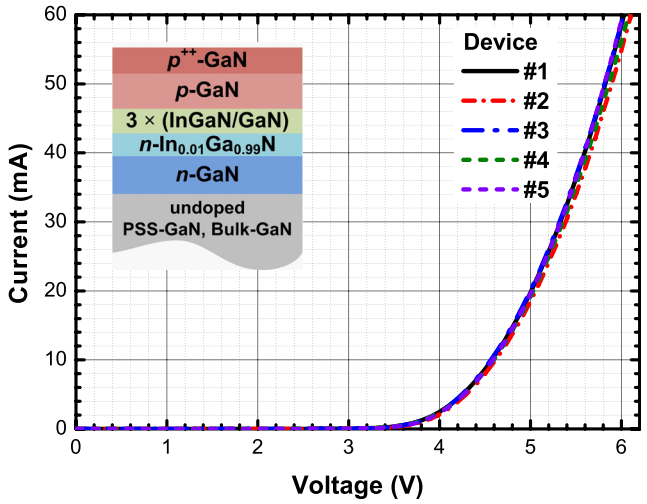

FIG. 2. Current-voltage characteristic curves measured on five different (11$\bar{2}$2) InGaN/GaN MQW LEDs. The inset displays the schematic illustration of the LED structures grown on PSS- and Bulk-GaN substrates.

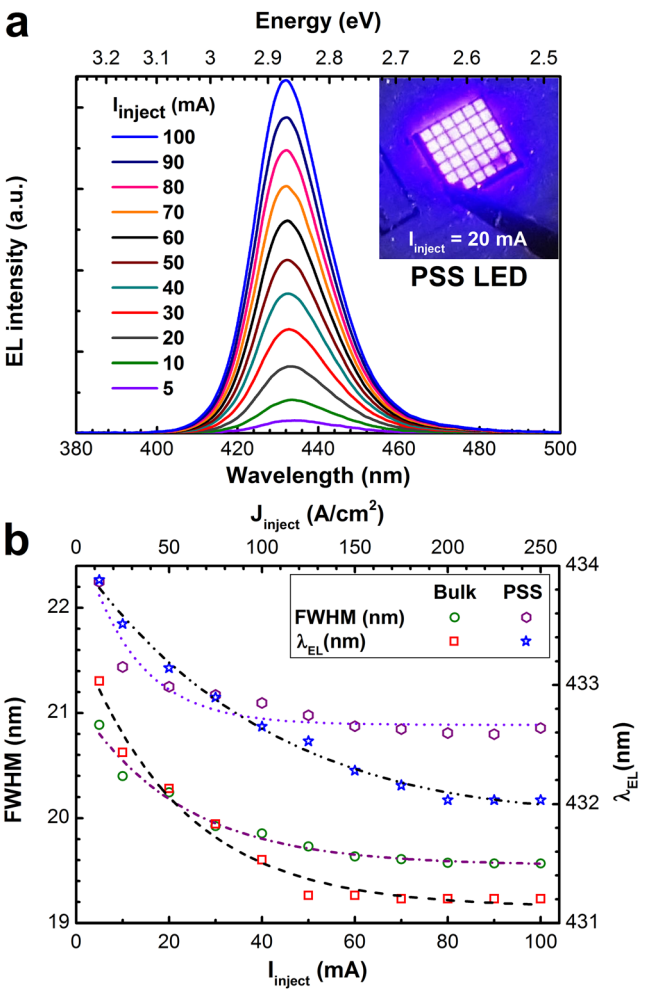

FIG. 3. (a) EL spectra of the 200 × 200 μm^2 PSS-LED as a function of I_{inject} measured on-wafer in pulsed mode. The inset shows a photograph of the PSS-LED displaying bright blue emission when $I_{inject} = 20$ mA is being injected to the device. (b) λ_{EL} and FWHM of the PSS- and Bulk-LEDs as a function of $I(J)_{inject}$.

To evaluate the stability of λ_{EL} and FWHM to I_{inject}, all the EL spectra of both LEDs were fitted using a Gaussian function. The estimated λ_{EL} and FWHM are plotted as a function of $I(J)_{inject}$ in Fig. 3(b). The PSS-/Bulk-LED starts to show EL emission at $\lambda_{EL} = 433.9/433.0$ nm with a FWHM of 22.2/20.9 nm. As I_{inject} increases up to ~50 mA, the λ_{EL} of both LEDs slightly blue-shifts and then stabilizes at higher I_{inject} with almost identical FWHM of 20.8/19.6 nm for the PSS-/Bulk-LED. The wavelength and FWHM variations are estimated to be about 1.8 nm and 1.4 nm for both LEDs, respectively. The blue-shift of 1.8 nm with increasing I_{inject} can be explained by the QCSE and band-filling effect.[1–3,23–28] For ~430 nm polar and ~425 nm (10$\bar{1}$1) InGaN LEDs,[29] blue-shifts of 3.5 nm and 1.5 nm have been reported, respectively. This smaller blue-shift value of the (10$\bar{1}$1) InGaN LED was attributed mainly to a weaker QCSE than the polar LED.[29] Based on theoretical calculations previously reported in the Ref. 3 for $In_{0.14}Ga_{0.86}N$/GaN QWs, the electric field across (11$\bar{2}$2) QWs caused by the spontaneous and piezoelectric polarizations in the wells and GaN barriers is roughly estimated to be about 3-times weaker than in polar QWs. The peak shift variation of the PSS- and Bulk-LEDs is in good agreement with values of ~1.3–2.0 nm previously reported for (11$\bar{2}$2) LEDs,[30,31] (10$\bar{1}$1) LEDs,[32] and (20$\bar{2}$1) LEDs.[33] Thus, these small peak shifts indicate a weak QCSE in semipolar InGaN QWs.

Figure 4 shows P_{opt} of the unpackaged PSS- and Bulk-LEDs measured in DC mode inside an integrating sphere as a function of I_{inject}. P_{opt} of the Bulk-LED was found to be about 2-times higher than the PSS-LED for measurements. For example, the P_{opt} at 20 mA was estimated to be 0.66 mW (the corresponding output power density (P_D) of 16.5 mW/mm^2) and 1.43 mW ($P_D = 35.8$ mW/mm^2) for the PSS- and Bulk-LEDs, respectively. These obtained P_{opt} at 20 mA are comparable to 1.8 mW ($P_D = 9.8$ mW/mm^2) obtained for 320 × 320 μm^2 packaged (11$\bar{2}$2) LEDs emitting at ~430 nm grown on Bulk-GaN substrates,[30] and 1.0 mW ($P_D = 1.5$ mW/mm^2) obtained for 1100 × 600 μm^2 unpackaged (11$\bar{2}$2) LEDs

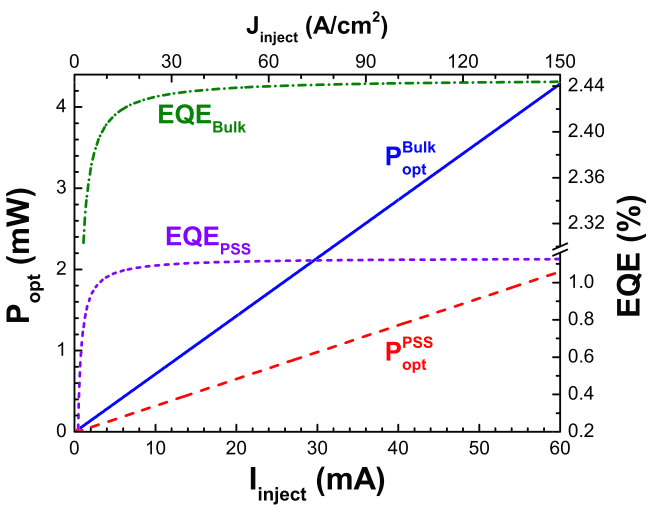

FIG. 4. P_{opt} and EQE of the unpackaged PSS- and Bulk-LEDs measured on-wafer in DC mode inside an integrating sphere as a function of I_{inject}.

emitting at ~441 nm grown directly on patterned *m*-plane sapphire.[31]

For both samples, EQE slowly increases and then stabilizes at $I_{inject} \geq 20$ mA. The increase of the EQE at low I_{inject} is due to a faster increase of the radiative recombination rate ($\sim n^2$) with increasing carrier density compared with the non-radiative processes ($\sim n$), e.g., Shockley-Read-Hall and other non-radiative recombination processes.[34–36] Peak EQE of the Bulk-/PSS-LED was estimated to be 2.45%/1.12%. These obtained peak EQE values are comparable with a peak EQE of 4.0% ($I_{inject} = 140$ mA, $J_{inject} = 140$ A/cm^2) reported for ~430 nm packaged ($11\bar{2}2$) LEDs ($320 \times 320\ \mu m^2$) grown on Bulk-GaN substrates,[30] and a peak EQE of 1.65% ($I_{inject} = 20$ mA, $J_{inject} = 3$ A/cm^2) reported for ~441 nm unpackaged ($11\bar{2}2$) LEDs ($1100 \times 600\ \mu m^2$) grown directly on patterned *m*-plane sapphire.[31]

The "efficiency droop" is a common issue in nitride LEDs,[37,38] which is caused by a non-radiative carrier loss mechanism that has small effect at low J_{inject} present in the active region, but becomes dominant at higher J_{inject}. The main reason of the droop is still under debate as many different mechanisms have been proposed including Auger recombination,[39–42] "carrier overflow"/poor hole-injection efficiency,[35,43,44] and density-activated defects.[45,46] Generally, the much smaller droop of nonpolar and semipolar LEDs in comparison with polar LEDs has been attributed to the weaker polarization fields.[30–33,47,48] However, it should be noted that low-efficiency polar LEDs also show a relatively small droop,[35,36] which has been attributed mainly to the strong effect of non-radiative recombination processes. Recently, Davies *et al.*[49] have suggested that the droop is inherent to the carrier density in InGaN QW structures and independent of crystal orientation. For the LEDs studied here with low luminescence efficiency (see Section III B), though no droop has been observed within the applied J_{inject} range, this can be attributed both to the weak QCSE and the non-radiative recombination processes.

B. Optical properties

Figure 5 shows TD-PL spectra of the PSS-LED ($E_{ex} = 3.06$ eV, $P_{ex} = 15$ W/cm^2). By using a Gaussian fit, the PL full-width at half maximum ($FWHM_{PL}$) values of this sample (and the Bulk-LED) were estimated to be 82.2/145.0 meV (76.4/138.0 meV) at 10/300 K. It should be noted that the spectrally integrated PL intensity (I_{PL}) of the PSS-LED is estimated to be about 1.4-/2.0-times higher than the Bulk-LED at 300/10 K. This difference in I_{PL} of both samples might be due to different internal reflections and light extraction. It has been found that the air void structures in LEDs grown on PSS-GaN substrates can lead to an enhanced light extraction resulting in an increase in I_{PL}.[19] The apparent internal quantum efficiency (IQE) was defined as the ratio of I_{300KPL}/I_{10KPL} in the weak excitation regime.[50] The IQE was estimated to be 10.0% and 20.3% for the PSS- and Bulk-LEDs, respectively. This lower IQE of the PSS-LED in comparison with the Bulk-LED is attributed mainly to the higher TDD and BSF density.

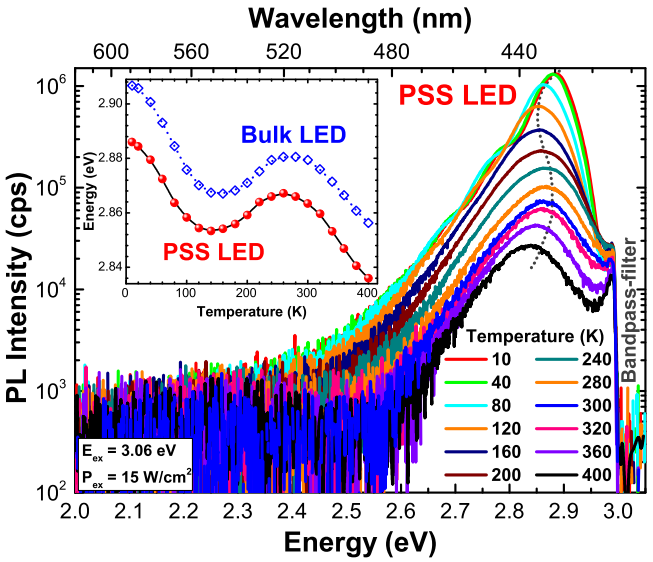

FIG. 5. TD-PL spectra of the PSS-LED measured with $E_{ex} = 3.06$ eV, $P_{ex} = 15$ W/cm^2. The inset shows the peak emission energy of the PSS-LED (●) and Bulk-LED (◇) as a function of temperature.

The inset of Fig. 5 shows the peak emission energy (E_{PL}) as a function of temperature of the PSS-LED ($P_{ex} = 15$ W/cm^2). E_{PL} follows an *S*-shaped temperature dependence. The QW emission energy starts to blue-shift at 160 K, then red-shifts at above 260 K. This can be explained via the hopping processes of excitons through localized states.[23,24,26–28] E_{PL} does not show any shift with different P_{ex} varying from 2 W/cm^2 to 15 W/cm^2. In the weak excitation regime employed here, no screening of the built-in field is expected. Thus, the *S*-shaped dependence indicates a strong exciton localization (ELOC) in the samples studied here. A similar finding has been previously reported for ($11\bar{2}2$) In_xGa_xN QWs ($0.13 \leq x \leq 0.35$).[27,28] To estimate the ELOC degree of both samples, a modified Varshni empirical expression[24,26–28] was used to fit the E_{PL} values within the temperature range of 160–400 K. The estimated ELOC degree of both samples was about 40 meV. This ELOC degree is higher than the values of ~12–24 meV previously reported for ~460 nm polar MQW.[26]

Figure 6 shows μ-PL maps ($30 \times 30\ \mu m^2$) of the PSS- and Bulk-LED samples at RT ($E_{ex} = 3.30$ eV, $P_{ex} = 150$ kW/cm^2). The E_{PL} maps of both samples are comparable with an average emission at 2.880 ± 0.007 eV. All images show stripes along the [$\bar{1}\bar{1}$23] inclined C′-direction with a periodicity of ~1–2 μm along the [1$\bar{1}$00] M-direction, which corresponds well to a typical periodicity of undulations along the M-direction observed for ($11\bar{2}2$) GaN.[22] As shown in Fig. 6(c), the $FWHM_{PL}$ distribution of the PSS-LED is not uniform, whereby the larger $FWHM_{PL}$ values are distributed along other stripes along the C′-direction with about ~5 μm periodicity (e.g., along arrow 3 in Fig. 6(c)). These stripes are believed to develop during coalescence from irregularities at the meeting facets of adjacent GaN template structures,[13,14] which normally result in a rough surface morphology resulting in a non-uniform luminescence of overgrown InGaN QWs.[21] In contrast, the $FWHM_{PL}$ map of the Bulk-LED is uniform. The average $FWHM_{PL}$ of the Bulk-LED was

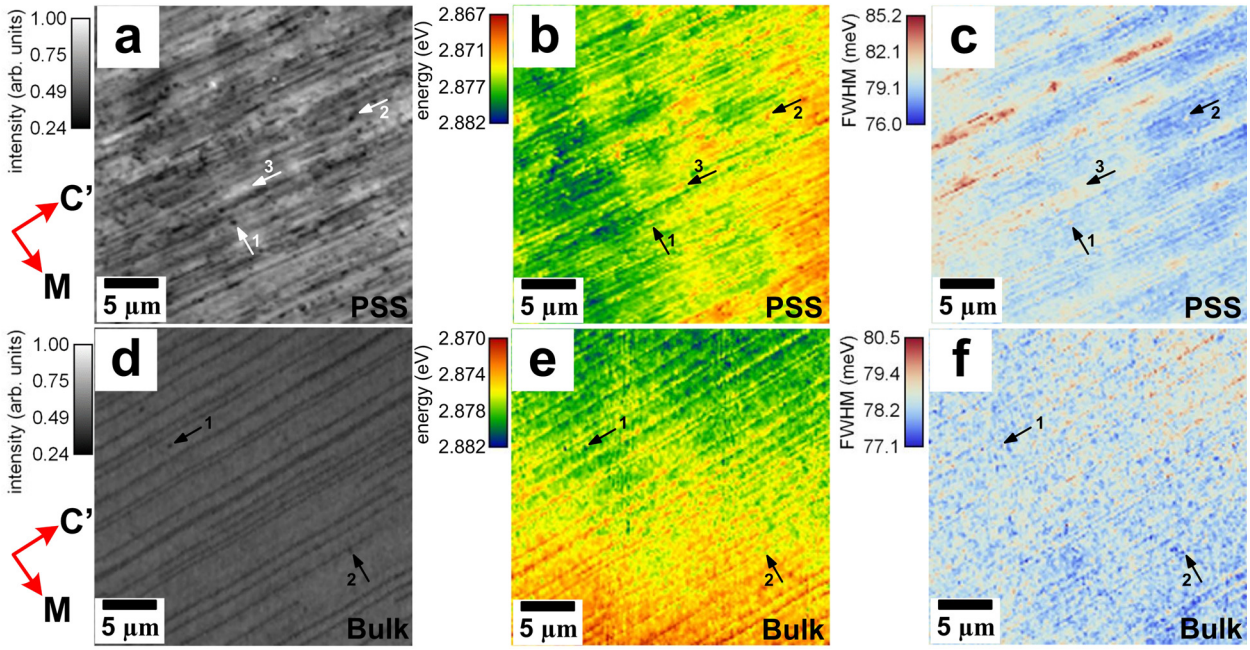

FIG. 6. μ-PL maps ($30 \times 30\ \mu m^2$) of the PSS- and Bulk-LEDs taken at RT ($E_{ex} = 3.30$ eV, $P_{ex} = 150$ kW/cm^2): intensity map plotted in the same intensity scale (a) PSS, (d) Bulk; emission energy map (b) PSS, (e) Bulk; FWHM map (c) PSS, (f) Bulk. Arrows 1 and 2 indicate a deep-dot area related to extended defects, while arrows 3 in (a)–(c) indicate a bright area without dot.

estimated to be 78.8 ± 1.7 meV slightly smaller than the PSS-LED of 80.6 ± 4.6 meV.

Despite the similar $E_{PL,}$ the absolute I_{PL} value of the PSS-LED is about 1.7-times higher than the Bulk-LED, consistent with the results obtained by macro-PL. For a direct comparison, the I_{PL} maps of both samples are plotted in the same intensity scale as shown in Figs. 6(a) and 6(d). The I_{PL} map of the Bulk-LED is more uniform than that of the PSS-LED. The PSS-LED shows a few bright spots (e.g., arrow 3 in Fig. 6(a)). The dark stripes observed in the I_{PL} maps of both samples can be attributed to misfit dislocations either under the QW active region or under the 100-nm-thick n-$In_{0.01}Ga_{0.99}N$ layer (as the layer thickness is close to the critical thickness[51]). It should be noted that the PSS-GaN template also shows such dark stripes.[13] Dark-dot related to extended defects (e.g., threading dislocations) can be clearly identified in the PL maps of both samples, as shown for examples as arrows 1 and 2 in Fig. 6. Consistent with the higher TDD, the dark-dot density of the PSS-LED ($\sim 2 \times 10^8$ cm^{-2}) is higher than that of the Bulk-LED ($\sim 1 \times 10^7$ cm^{-2}). The dark-dot areas of both samples have lower I_{PL} than the non-dot areas. As shown for instance by the arrows 1 and 2 in Figs. 6(a)–6(c), dark dots of the PSS-LED are generally red-shifted and have a broader FWHM with respect to their surrounding. Vice versa, dark dots in the Bulk-LED (Figs. 6(d)–6(f)) are blue-shifted and have a narrower FWHM with respect to their surrounding. The higher In-incorporation InGaN regions, e.g., the red-shifted areas should act as ELOC areas in which diffusing carriers can be trapped.[23–28] The ELOC areas in the PSS-LED are darker, which can explain its lower IQE in comparison with the Bulk-LED where ELOC areas are brighter.

C. Discussion

The lower P_{opt} of the PSS-LED compared to the Bulk-LED is contrary to the I_{PL} values measured by PL, whereby the PSS-LED is brighter. It should be noted that in an MQW structure under PL excitation, electron-hole pairs are generated in the whole structure, whereas under EL excitation, the generated carriers are mostly distributed in the QW nearest the p-layer.[44,52] For InGaN QW structures, it is well-known that TDs strongly affect IQE as they can act as non-radiative recombination centres.[25,53–55] However, it has been found that a strong ELOC can effectively reduce the QW excitons from being trapped into TDs, resulting in an enhanced luminescence efficiency from InGaN based devices.[23,25–27] Despite the strong ELOC (Fig. 5), the IQE values of the PSS-LED (and Bulk-LED) are much smaller than values reported for polar samples, which were grown on either higher- or comparable-TDD GaN/sapphire substrates.[26,27,54] The lower IQE values of these $(11\bar{2}2)$ QWs can be attributed to higher concentrations of unintentional impurities and point defects than in polar samples.[27,57,58] The efficiency of $(11\bar{2}2)$ QWs is therefore expected to significantly increase by lowering these concentrations. A further growth optimization is also essential to reduce the density of misfit dislocations (Figs. 6(a) and 6(d)).

For the PSS-LED, despite the strong ELOC, the ELOC areas were found to correlate with TDs reducing luminescence intensity (Figs. 6(a)–6(c)). The higher TDD of the PSS-LED causes the lower IQE than the Bulk-LED. It should be noted that the patterned sapphire substrates enhance light extraction.[19] Even though the measured I_{PL} is larger for the PSS-LED than for the Bulk-LED, the emitted intensity is actually larger for the Bulk-LED.

In EL measurements, P_{opt} of an LED is governed by the IQE, injection efficiency, and light extraction efficiency. If the LED has a high density of non-radiative recombination centres (e.g., high TDD), then this LED will have a lower density of electron-hole pairs (due to the lower hole injection efficiency) to recombine within the active region resulting in a lower P_{opt}. For the PSS-LED, though the patterned sapphire enhances its light extraction, the higher TDD acts as a non-radiative recombination centre resulting in the lower P_{opt}.[45,46] The high BSF density of the PSS-LED may act as a non-radiative recombination centre that may further reduce P_{opt}.[56] Additionally, the rough surface morphology of the PSS-LED (Fig. 1) is another issue as it can cause nonuniform carrier distribution[21,44] and compositional fluctuations.[21] It has been previously found that polished PSS-GaN substrates can strongly enhance the luminescence uniformity of QWs and the performance of PSS-LEDs.[21]

The internal absorption has been found to be significant in nitrides for emission energy below the GaN band-edge due to background doping, leading to an increase in electronic transitions between donor-acceptor levels and structural defects.[59–61] For example, the absorption coefficient at 450 nm of Bulk-GaN substrates has been found to increase with increasing unintentional O-impurity concentration.[60,61] The internal absorption in the 6-μm-thick PSS-GaN substrate in comparison with the 300-μm-thick Bulk-GaN substrate might be higher due to the higher O-impurity concentration of about $1.0 \times 10^{17}\,cm^{-3}$ (Ref. 13) ($<7 \times 10^{15}\,cm^{-3}$ in the Bulk-GaN[6]). However, this internal absorption can be neglected due to the much thinner PSS-GaN substrate.

To conclude, the lower IQE of the PSS-LED in comparison with the Bulk-LED is attributed mainly to the higher TDD. The rough surface morphology of the PSS-GaN substrate might cause nonuniform carrier distribution. Additionally, the TDD and BSFs might cause current leakage and lateral current spreading issues. All these issues can reduce the performance of the PSS-LED. Thus, a further reduction of the TDD and BSF density and a smooth morphology of the PSS-GaN substrate are expected to strongly enhance the performance of overgrown LEDs.

IV. CONCLUSIONS

The optical properties and device performance of unpackaged InGaN/GaN LEDs emitting at ~430 nm grown simultaneously on a bulk semipolar $(11\bar{2}2)$ GaN substrate (Bulk-GaN) and a $(11\bar{2}2)$ GaN template created on patterned $(10\bar{1}2)$ *r*-plane sapphire substrate (PSS-GaN) have been compared. The LED grown on PSS-GaN substrate has about two-times lower output power and internal quantum efficiency values compared to the LED grown on Bulk-GaN substrate. These lower values were attributed to higher densities of threading dislocations and basal stacking faults of the LED grown on rough surface PSS-GaN substrate, which might cause current leakage and current spreading, as well as create non-radiative recombination centres. A further reduction of the defect densities and impurity concentrations, as well as a smooth surface morphology of the PSS-GaN substrates are expected to strongly enhance the performance of overgrown LEDs.

ACKNOWLEDGMENTS

This work was financially supported by the EU-FP7 ALIGHT project, under Agreement No. FP7-280587.

[1]F. Bernardini, V. Fiorentini, and D. Vanderbilt, Phys. Rev. B **56**, R10024 (1997).
[2]T. Takeuchi, H. Amano, and I. Akasaki, Jpn. J. Appl. Phys., Part 1 **39**, 413 (2000).
[3]A. E. Romanov, T. J. Baker, S. Nakamura, and J. S. Speck, J. Appl. Phys. **100**, 023522 (2006).
[4]H. Sato, A. Tyagi, H. Zhong, N. Fellows, R. B. Chung, M. Saito, K. Fujito, J. S. Speck, S. P. DenBaars, and S. Nakamura, Phys. Status Solidi RRL **1**, 162 (2007).
[5]H. Sato, R. B. Chung, H. Hirasawa, N. Fellows, H. Masui, F. Wu, M. Saito, K. Fujito, J. S. Speck, S. P. DenBaars, and S. Nakamura, Appl. Phys. Lett. **92**, 221110 (2008).
[6]K. Fujito, S. Kubo, and I. Fujimura, MRS Bull. **34**, 313 (2009).
[7]T. J. Baker, B. A. Haskell, F. Wu, J. S. Speck, and S. Nakamura, Jpn. J. Appl. Phys., Part 2 **45**, L154 (2006).
[8]T. Wernicke, C. Netzel, M. Weyers, and M. Kneissl, Phys. Status Solidi C **5**, 1815 (2008).
[9]S. Y. Bae, D. S. Lee, B. H. Kong, H. K. Cho, J. F. Kaeding, S. Nakamura, S. P. DenBaars, and J. S. Speck, Curr. Appl. Phys. **11**, 954 (2011).
[10]Z. Bougrioua, M. Laügt, P. Vennégués, I. Cestier, T. Gühne, E. Frayssinet, P. Gibart, and M. Leroux, Phys. Status Solidi A **204**, 282 (2007).
[11]T. Gühne, Z. Bougrioua, P. Vennégués, M. Leroux, and M. Albrecht, J. Appl. Phys. **101**, 113101 (2007).
[12]N. Okada, A. Kurisu, K. Murakami, and K. Tadatomo, Appl. Phys. Express **2**, 091001 (2009).
[13]F. Brunner, U. Zeimer, F. Edokam, W. John, D. Prasai, O. Krüger, and M. Weyers, Phys. Status Solidi B **252**, 1189 (2015).
[14]Y. Han, M. Caliebe, F. Hage, Q. Ramasse, M. Pristovsek, T. Zhu, F. Scholz, and C. Humphreys, Phys. Status Solidi B **253**, 834 (2016).
[15]See http://www.alight-project.eu for the ALIGHT project description.
[16]H. Gao, F. Yan, Y. Zhang, J. Li, Y. Zeng, and G. Wang, J. Appl. Phys. **103**, 014314 (2008).
[17]Y. Narukawa, M. Ichikawa, D. Sanga, M. Sano, and T. Mukai, J. Phys. D: Appl. Phys. **43**, 354002 (2010).
[18]X.-F. Li, S.-W. Huang, H.-Y. Lin, C.-Y. Lu, S.-F. Yang, C.-C. Sun, and C.-Y. Liu, Opt. Mater. Express **5**, 1784 (2015).
[19]N. Okada, K. Uchida, S. Miyoshi, and K. Tadatomo, Phys. Status Solidi A **209**, 469 (2012).
[20]B. Leung, Y. Zhang, C. D. Yerino, J. Han, Q. Sun, Z. Chen, S. Lester, K. Y. Liao, and Y. L. Li, Semicond. Sci. Technol. **27**, 024016 (2012).
[21]D. V. Dinh, M. Akhter, S. Presa, G. Kozlowski, D. O'Mahony, P. P. Maaskant, F. Brunner, M. Caliebe, M. Weyers, F. Scholz, B. Corbett, and P. J. Parbrook, Phys. Status Solidi A **212**, 2196 (2015).
[22]S. Ploch, T. Wernicke, D. V. Dinh, M. Pristovsek, and M. Kneissl, J. Appl. Phys. **111**, 033526 (2012).
[23]S. Chichibu, T. Azuhata, T. Sota, and S. Nakamura, Appl. Phys. Lett. **69**, 4188 (1996).
[24]P. G. Eliseev, P. Perlin, J. Lee, and M. Osiński, Appl. Phys. Lett. **71**, 569 (1997).
[25]S. F. Chichibu, H. Marchand, M. S. Minsky, S. Keller, P. T. Fini, J. P. Ibbetson, S. B. Fleischer, J. S. Speck, J. E. Bowers, E. Hu, U. K. Mishra, S. P. DenBaarrs, T. Deguchi, T. Sota, and S. Nakamura, Appl. Phys. Lett. **74**, 1460 (1999).
[26]H. Wang, Z. Ji, S. Qu, G. Wang, Y. Jiang, B. Liu, X. Xu, and H. Mino, Opt. Express **20**, 3932 (2012).
[27]D. V. Dinh, S. Presa, P. P. Maaskant, B. Corbett, and P. J. Parbrook, Semicond. Sci. Technol. **31**, 085006 (2016).
[28]D. V. Dinh, F. Brunner, M. Weyers, B. Corbett, and P. J. Parbrook, J. Appl. Phys. **120**, 055705 (2016).
[29]T. Wunderer, P. Bruckner, B. Neubert, F. Scholz, M. Feneberg, F. Lipski, M. Schirra, and K. Thonke, Appl. Phys. Lett. **89**, 041121 (2006).
[30]M. Funato, M. Ueda, Y. Kawakami, Y. Narukawa, T. Kosugi, M. Takahashi, and T. Mukai, Jpn. J. Appl. Phys., Part 2 **45**, L659 (2006).
[31]D. S. Kim, S. Lee, D. Y. Kim, S. K. Sharma, S. M. Hwang, and Y. G. Seo, Appl. Phys. Lett. **103**, 021111 (2013).
[32]C.-H. Chiu, D.-W. Lin, C.-C. Lin, Z.-Yu. Li, W.-T. Chang, H.-W. Hsu, H.-C. Kuo, T.-C. Lu, S.-C. Wang, W.-T. Liao, T. Tanikawa, Y. Honda, M. Yamaguchi, and N. Sawaki, Appl. Phys. Express **4**, 012105 (2011).

[33]C.-C. Pan, S. Tanaka, F. Wu, Y. Zhao, J. S. Speck, S. Nakamura, S. P. DenBaars, and D. Feezell, Appl. Phys. Express **5**, 062103 (2012).
[34]S. F. Chichibu, A. Uedono, T. Onuma, B. A. Haskell, A. Chakraborty, T. Koyama, P. T. Fini, S. Keller, S. P. Denbaars, J. S. Speck, U. K. Mishra, S. Nakamura, S. Yamaguchi, S. Kamiyama, H. Amano, I. Akasaki, J. Han, and T. Sota, Nat. Mater. **5**, 810 (2006).
[35]Y. Lin, Y. Zhang, Z. Liu, L. Su, J. Zhang, T. Wei, and Z. Chen, Appl. Phys. Lett. **101**, 252103 (2012).
[36]W. Liu, D. Zhao, D. Jiang, P. Chen, Z. Liu, J. Zhu, X. Li, F. Liang, J. Liu, and L. Zhang, J. Phys. D: Appl. Phys. **49**, 145104 (2016).
[37]J. Piprek, Phys. Status Solidi A **207**, 2217 (2010).
[38]J. Cho, E. F. Schubert, and J. K. Kim, Laser Photonics Rev. **7**, 408 (2013).
[39]Y. C. Shen, G. O. Mueller, S. Watanabe, N. F. Gardner, A. Munkholm, and M. R. Krames, Appl. Phys. Lett. **91**, 141101 (2007).
[40]E. Kioupakis, P. Rinke, K. T. Delaney, and C. G. Van de Walle, Appl. Phys. Lett. **98**, 161107 (2011).
[41]H.-Y. Ryu, D.-S. Shin, and J.-I. Shim, Appl. Phys. Lett. **100**, 131109 (2012).
[42]J. Iveland, L. Martinelli, J. Peretti, J. S. Speck, and C. Weisbuch, Phys. Rev. Lett. **110**, 177406 (2013).
[43]M.-H. Kim, M. F. Schubert, Q. Dai, J. K. Kim, E. F. Schubert, J. Piprek, and Y. Park, Appl. Phys. Lett. **91**, 183507 (2007).
[44]A. David, M. J. Grundmann, J. F. Kaeding, N. F. Gardner, T. G. Mihopoulos, and M. R. Krames, Appl. Phys. Lett. **92**, 053502 (2008).
[45]M. F. Schubert, S. Chhajed, J. K. Kim, E. F. Schubert, D. D. Koleske, M. H. Crawford, S. R. Lee, A. J. Fischer, G. Thaler, and M. A. Banas, Appl. Phys. Lett. **91**, 231114 (2007).
[46]J. Hader, J. V. Moloney, and S. W. Koch, Appl. Phys. Lett. **96**, 221106 (2010).
[47]D. F. Feezell, J. S. Speck, S. P. DenBaars, and S. Nakamura, J. Disp. Technol. **9**, 190 (2013).
[48]T. Detchprohm, M. Zhu, Y. Li, Y. Xia, C. Wetzel, E. A. Preble, L. Liu, T. Paskova, and D. Hanser, Appl. Phys. Lett. **92**, 241109 (2008).
[49]M. J. Davies, P. Dawson, S. Hammersley, T. Zhu, M. J. Kappers, C. J. Humphreys, and R. A. Oliver, Appl. Phys. Lett. **108**, 252101 (2016).
[50]Y. Narukawa, Y. Kawakami, S. Fujita, and S. Nakamura, Phys. Rev. B **59**, 10283 (1999).
[51]P. S. Hsu, E. C. Young, A. E. Romanov, K. Fujito, S. P. DenBaars, S. Nakamura, and J. S. Speck, Appl. Phys. Lett. **99**, 081912 (2011).
[52]M. Peter, A. Laubsch, P. Stauss, A. Walter, J. Baur, and B. Hahn, Phys. Status Solidi C **5**, 2050 (2008).
[53]J. Abell and T. D. Moustakas, Appl. Phys. Lett. **92**, 091901 (2008).
[54]Q. Dai, M. F. Schubert, M. H. Kim, J. K. Kim, E. F. Schubert, D. D. Koleske, M. H. Crawford, S. R. Lee, A. J. Fischer, G. Thaler, and M. A. Banas, Appl. Phys. Lett. **94**, 111109 (2009).
[55]I.-L. Lu, Y.-R. Wu, and J. Singh, J. App. Phys. **108**, 124508 (2010).
[56]F. Wu, Y.-D. Lin, A. Chakraborty, H. Ohta, S. P. DenBaars, S. Nakamura, and J. S. Speck, Appl. Phys. Lett. **96**, 231912 (2010).
[57]S. C. Cruz, S. Keller, T. E. Mates, U. K. Mishra, and S. P. DenBaars, J. Cryst. Growth **311**, 3817 (2009).
[58]S. F. Chichibu, A. Uedono, T. Onuma, S. P. DenBaars, U. K. Mishra, J. S. Speck, and S. Nakamura, Mater. Sci. Forum **590**, 233 (2008).
[59]O. Ambacher, W. Rieger, P. Ansmann, H. Angerer, T. D. Moustakas, and M. Stutzmann, Solid State Commun. **97**, 365 (1996).
[60]E. R. Letts, T. Hashimoto, S. Hoff, D. Key, K. Male, and M. Michaels, J. Cryst. Growth **403**, 3 (2014).
[61]S. Pimputkar, S. Suihkonen, M. Imade, Y. Mori, J. S. Speck, and S. Nakamura, J. Cryst. Growth **432**, 49 (2015).